

Single-stage liquid-phase synthesis of methyl isobutyl ketone under mild conditions

Ferry Winter, A. Jos van Dillen, Krijn P. de Jong*

*Department of Inorganic Chemistry and Catalysis, Debye Institute, Utrecht University,
P.O. Box 80 083, 3508 TB Utrecht, The Netherlands*

Received 13 April 2004; accepted 26 April 2004

Available online 2 July 2004

Abstract

In this study, a catalyst mixture of activated Mg/Al hydrotalcite as solid base and Pd on carbon nanofibers was investigated for the single-stage liquid-phase synthesis of methyl isobutyl ketone (MIBK) from acetone and H₂ at 313 K and H₂ pressures of 1–20 bar. With this catalyst system acetone and H₂ are selectively converted into MIBK in a single reactor, even at 1.2 bar H₂. Although the hydrogenation of one of the intermediates, mesityl oxide (MO), at 1.2 bar suffers from severe mass transfer limitations in H₂, the catalytic activity in the single-stage synthesis is stable over several hours if the steady-state concentration of MO is kept low. Under the presented conditions the dehydration reaction of diacetone alcohol to MO is rate limiting in the production of MIBK.

© 2004 Elsevier B.V. All rights reserved.

Keywords: Carbon nanofibers; CNF; Palladium catalyst; Platinum catalyst; Hydrotalcite; Mesityl oxide; Methyl isobutyl ketone; MIBK

1. Introduction

Methyl isobutyl ketone (MIBK) is an industrially important chemical, mainly used as a coating solvent. It is the third largest tonnage product formed from acetone and is mainly produced via a conventional three-step process, wherein starting from acetone the three reactions are executed separately (Fig. 1). The first step consists of the aldol condensation of acetone to form diacetone alcohol (DAA). In a sequential step DAA is dehydrated to mesityl oxide (MO). In the third step, MIBK is formed by selective hydrogenation of the C=C bond of MO. The first two steps are base and acid catalysed reactions, respectively, the third step is generally catalysed by supported noble metals.

The high costs for the conventional three-step process relate to the yields of the first two steps being controlled by the thermodynamic equilibria of these reactions. The equilibrium of the condensation of acetone shifts to DAA at lower reaction temperatures, whereas for the dehydration step the equilibrium shifts to MO at higher reaction temperatures [1–4]. To deal with the thermodynamic constraints, single-stage processes have been developed to

convert acetone and hydrogen directly into MIBK. Several catalytic systems containing condensation, dehydration and hydrogenation functionalities have been investigated for the single-stage process, e.g., Pd on ion-exchange resin [5], Pd or Pt on ZSM-5 [6–8], Pd/Nb₂O₅/SiO₂ [9,10], Ni/γ-Al₂O₃ [11] and Ni or Pd on MgO [12,13]. The single-stage processes as developed or proposed up to now still require high reaction temperatures and pressures, and side-reactions occur, in particular hydrogenation of acetone to 2-propanol and probably polymerization. As a consequence, the selectivity of the process is lowered and the catalysts deactivate [14–17].

Several studies have been reported on the use of hydrotalcite-based catalyst systems for the single-stage production of MIBK [15,16,18–20], in which the process is mainly performed at high temperatures and/or hydrogen pressures. In these studies, the actual condensation catalyst is a mixed oxide obtained by calcination of the hydrotalcite. Recently, extending the pioneering work of Tichit and co-workers [21–24] our group developed a highly active catalyst for the liquid-phase condensation of acetone at low temperatures, i.e., activated Mg–Al hydrotalcite (HT) [25,26]. Furthermore, this catalyst showed dehydration functionality of DAA to MO already at room temperature [2,26].

* Corresponding author. Tel.: +31 30 2536762; fax: +31 30 2511027.
E-mail address: k.p.dejong@chem.uu.nl (K.P. de Jong).

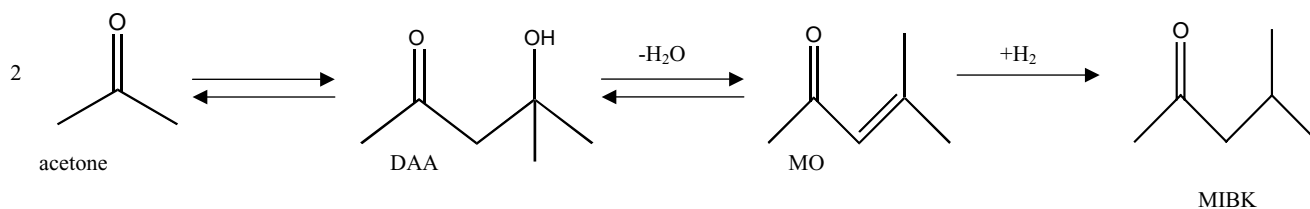


Fig. 1. Reaction scheme of the self-condensation of acetone to diacetone alcohol (DAA), dehydration of DAA to mesityl oxide (MO) and followed by selective hydrogenation to methyl isobutyl ketone (MIBK).

Earlier studies reported in literature on the hydrogenation of MO to MIBK showed that at higher temperatures the reaction proceeds with appreciable initial rates [27,28]. However, with the catalysts explored up to now at low pressure and temperature full conversion of MO to MIBK is not attained due to deactivation [29]. For hydrogenation of α,β -unsaturated ketones and aldehydes, palladium-based catalysts, especially Pd/C catalysts, exhibit the best performance in the hydrogenation of the olefinic bond [15,30]. As a promising alternative for activated carbon we used carbon nanofibers (CNF) as the support material, because of their high mechanical strength, high surface area and accessibility, tuneable surface properties, their purity and the absence of micropores [31].

In this work we studied the formation of DAA and MO from acetone using activated HT. Furthermore, a palladium on CNF catalyst (Pd/CNF) was investigated in the hydrogenation of MO at H₂ pressures ranging between 1 and 20 bar and with different MO concentrations. An exploratory study was conducted on the performance of this Pd/CNF catalyst in comparison with other supported palladium catalysts, i.e., Pd on SiO₂ (Pd/SiO₂) and Pd on graphite (Pd/G), and with a platinum supported on CNF catalyst (Pt/CNF). Finally, the single-stage conversion of acetone and H₂ into MIBK under mild conditions was studied using a catalyst mixture of activated HT and the Pd/CNF catalyst.

2. Experimental

2.1. Preparation of hydrotalcite materials

HT with a Mg/Al ratio of 2 was prepared via co-precipitation [32]. To an aqueous solution (70 ml) containing 0.35 mol NaOH (Merck) and 0.09 mol Na₂CO₃ (Acros) an aqueous solution (45 ml) of 0.1 mol Mg(NO₃)₂·6H₂O (Acros) and 0.05 mol Al(NO₃)₂·9H₂O (Merck) was added. The resulting white suspension was heated to 333 K for 24 h under vigorous stirring, after which the precipitate was filtered off and washed extensively. The sample, further designated as HT-CO₃, was dried for 24 h at 393 K.

HT-CO₃ was activated using the procedure of Roelofs et al. [33]. HT-CO₃ was heated to 723 K (10 K min⁻¹) in a nitrogen flow for 8 h (HT_{calc}). HT_{calc} was rehydrated in decarbonated water for 1 h under nitrogen atmosphere, filtered off and washed with ethanol to obtain a relatively high amount of accessible basic sites (HT_{act}).

2.2. Growth of carbon nanofibers

CNF were grown out of a commercial 57 wt.% Ni/SiO₂ catalyst (Engelhard Ni5270P, calcined at 648 K for three hours) from syngas [34,35]. About one gram of calcined Ni/SiO₂ was first reduced at 873 K in a fixed bed reactor for 2 h in a 20% H₂/N₂ flow (400 ml min⁻¹). Next, the temperature was decreased to 773 K and a mixture of CO (80 ml min⁻¹), H₂ (30 ml min⁻¹) and N₂ (290 ml min⁻¹) was passed through the catalyst bed for 20 h. The reactor content was refluxed for 1.5 h in a KOH solution (1 M) and thoroughly washed in order to remove the silica support. Next, the fibers were treated for 2 h in boiling concentrated nitric acid to remove exposed nickel and to introduce adsorption sites, cooled to room temperature, filtered off, thoroughly washed with demineralised water and dried at 393 K for 24 h.

2.3. Preparation of palladium and platinum supported catalysts

Pd or Pt was deposited on the carbon supports via an ion adsorption method, earlier applied by Hoogenraad [36]. Typically, 5 g of oxidized CNF or graphite (Lonza, HSAG100) was suspended in 100 ml demineralised water. The pH of the suspension was adjusted at a value between 5 and 6 by adding ammonium hydroxide solution (25%). Subsequently, an aqueous solution of Pd(NH₃)₄(NO₃)₂ (Alfa Aesar) or Pt(NH₃)₄(NO₃)₂ (Aldrich) was added and the resulting suspension was stirred for 20 h at room temperature under N₂ atmosphere. The catalyst precursor was filtered off under N₂ flow, washed and dried at 353 K for 20 h in N₂ flow. The Pd catalyst precursors were reduced in hydrogen flow at 523 K (5 K min⁻¹) for 2 h, whereas the Pt catalyst precursor was reduced at 473 K (2 K min⁻¹) in hydrogen flow for 3 h. A 3 wt.% Pd on SiO₂ catalyst obtained from Engelhard (Q500-189, unreduced sample) was reduced in hydrogen flow at 523 K for 2 h (5 K min⁻¹).

2.4. Catalyst characterization

Powder X-ray diffraction (XRD) patterns were measured using an Enraf-Nonius CPS 120 powder diffraction apparatus with Co K α radiation ($\lambda = 1.789 \text{ \AA}$). N₂ physisorption measurements were performed using a Micromeritics ASAP 2400 analyser. When micropores are present, the surface area

calculated with the *t*-method is reported instead of the BET surface area. Volumetric CO₂ adsorption measurements in the range 0–100 mbar were executed at 273 K with a Micromeritics ASAP 2010C apparatus after drying the samples at 393 K in vacuo for at least 20 h. The total amount of accessible sites was determined taking the amount of CO₂ chemisorbed to zero pressure by extrapolation of the linear part of the uptake isotherm. Hydrogen chemisorption data were recorded using a Micromeritics ASAP 2010C apparatus. Prior to the chemisorption measurements at 343 K for the Pd samples and 307 K for the Pt catalyst, samples were dried in vacuo at 393 K for 16 h, reduced in H₂ flow at 473 K for 2 h (5 K min⁻¹) and degassed for two hours at the reduction temperature. The H/M ratios are based on the amount of hydrogen adsorbed by extrapolating the linear part of the isotherm of the total amount of adsorbed hydrogen to zero pressure. TEM images to assess the metal particle size were obtained with a Philips CM-200 FEG TEM operating at 200 kV. Samples were, after an ultrasonic treatment in butanol, dispersed on a holey carbon film. A Philips XL30FEG electron microscope was used to obtain SEM images. ICP analyses to determine metal loadings were performed using a Thermo Jarrel Ash Atom Scan 16 apparatus. After crushing and suspending in ethanol, the catalyst particle size distribution was measured with an optical particle sizer Accusizer Model 770, capable of detecting particles in the range of 1–500 μm.

2.5. Catalytic reaction procedures

Condensation and dehydration to MO experiments were performed under N₂ atmosphere with 0.30 g of activated HT catalyst. MO hydrogenation experiments were performed in a semi-batch slurry reactor operating at a constant pressure of 1.2 bar H₂ at 313 K [37]. The set-up consisted of a thermostatted stirred double-walled glass reactor, equipped with baffles and a gas-tight mechanical stirrer. For a typical hydrogenation experiment, 50 mg of crushed hydrogenation

catalyst was kept in 1.2 bar H₂ for one hour, after which it was added to a solution containing 120 ml of acetone or ethanol, 6 g iso-octane as an internal standard (99.5% pure) and MO (Acros, 99% α- and β-isomer (ratio 1:13), purified by distillation) at 313 K. During the reaction the hydrogen consumption was monitored by an electronic mass flow controller. For the single-stage synthesis of MIBK at 331 K and 1.2 bar H₂ a mixture of 0.3 g HT_{act} and 0.2 g Pd/CNF was used. MO hydrogenation experiments at 10 and 20 bar H₂ were performed in a 11 Parr reactor. Typically, 275 mg of crushed catalyst was suspended in 670 ml of ethanol or acetone at 313 K, after which a second solution containing 80 ml of ethanol or acetone and the desired amount of MO was added. Next, the reactor was filled with H₂ and pressurized. Aliquots of 1 ml were taken from the reaction mixture during reaction and analysed using a Chrompack CP 9001 GC provided with a Chrompack CP 9050 autosampler.

3. Results and discussion

3.1. Characterization of the hydrotalcite

The XRD pattern of HT-CO₃ shows the characteristics of a crystalline layered structure (Fig. 2a). By heating the sample up to 723 K, the layered structure is destroyed and a mixed oxide phase is present as can be concluded from XRD (Fig. 2b). This heat treatment causes a large increase in surface area as well as in micropore and mesopore volume and a lowering of the average pore diameter (Table 1) [38]. Upon reconstructing the HT structure by rehydrating HT_{calc} in CO₂-free water, the micropores disappear and the average pore diameter increases. The HT structure is restored to a large extent as can be concluded from XRD (Fig. 2c), although line broadening is apparent in the XRD pattern of HT_{act} when compared to that of HT-CO₃.

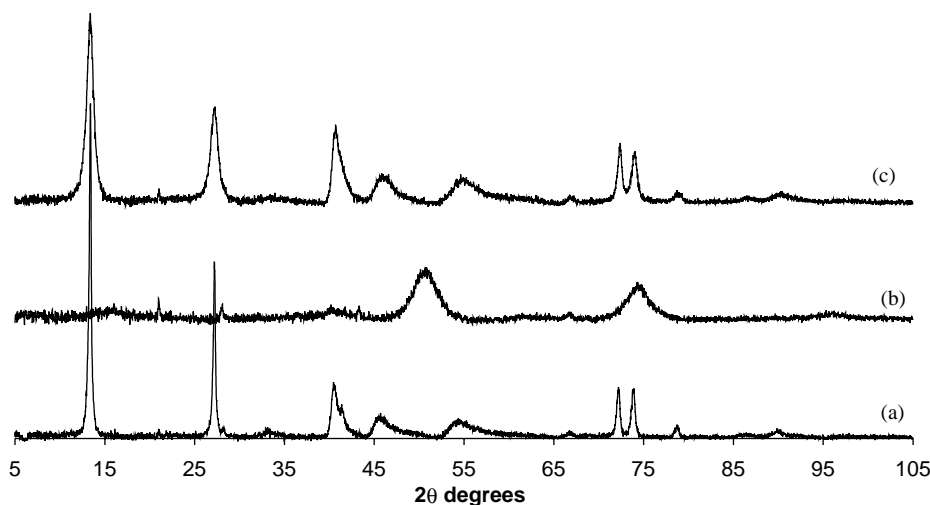


Fig. 2. XRD patterns of (a) HT-CO₃, (b) HT_{calc} and (c) HT_{act}.

Table 1
Results from N₂-physisorption of HT samples

Sample	Surface area (m ² g ⁻¹)	Total pore volume (ml g ⁻¹)	Micropore volume (ml g ⁻¹)	Average pore diameter (nm)
HT-CO ₃	58	0.37	0.00	25
HT _{calc}	109 ^a	0.54	0.01	11
HT _{act}	132	0.61	0.00	19

^a Surface area calculated with *t*-method.

Volumetric CO₂-adsorption measurements were performed to get information about the total amount of accessible active basic sites of HT_{act}. With the sample prepared as described, typically 6.6 ml STP CO₂ g_{HT}⁻¹ was found, corresponding to 0.29 mmol g_{HT}⁻¹ of basic sites. According to these results, we calculated that these sites represent about 6 mol% of the total amount of aluminium present in the structure of HT. This is in line with the conclusions stated by Roelofs et al. [25], that only the active sites at the edge area of the stacked platelets are accessible.

3.2. Characterization of the support material

In Fig. 3 an SEM image of CNF is displayed. The fibers are tightly interwoven and the skeins of the fibers form a porous structure. The diameter of the fibers is in the range of 20–80 nm. XRD and TEM showed that the graphite-like structure of CNF had not been affected after removal of the growth catalyst and the activation treatment with nitric acid

Table 2
Results from N₂ physisorption

Sample	Surface area (m ² g ⁻¹)	Total pore volume (ml g ⁻¹)	Micropore volume (ml g ⁻¹)
Oxidized CNF	137	0.38	0.00
Graphite	111	0.25	0.00
Pd/SiO ₂	278 ^a	0.93	0.02

^a Surface area calculated with *t*-method.

needed for applying the metal precursor. Graphite shows platelets with only the external surface accessible for large molecules (not shown). The graphite platelets are randomly stacked to form a house of cards structure with a meso- and macro pore structure.

The results of N₂-physisorption of the support materials are given in Table 2. CNF as well as the graphite support show a much lower surface area and pore volume than the Pd/SiO₂ material. No micropores were present in the CNF and graphite support materials, whereas micropores were observed with Pd/SiO₂.

3.3. Characterization of palladium and platinum supported catalysts

In Table 3 the characterisation results of the various hydrogenation catalysts are presented. After reduction at 523 K of the Pd/CNF catalyst, TEM examination shows palladium particles on the fibers of about 1–4 nm (Fig. 4). Examination

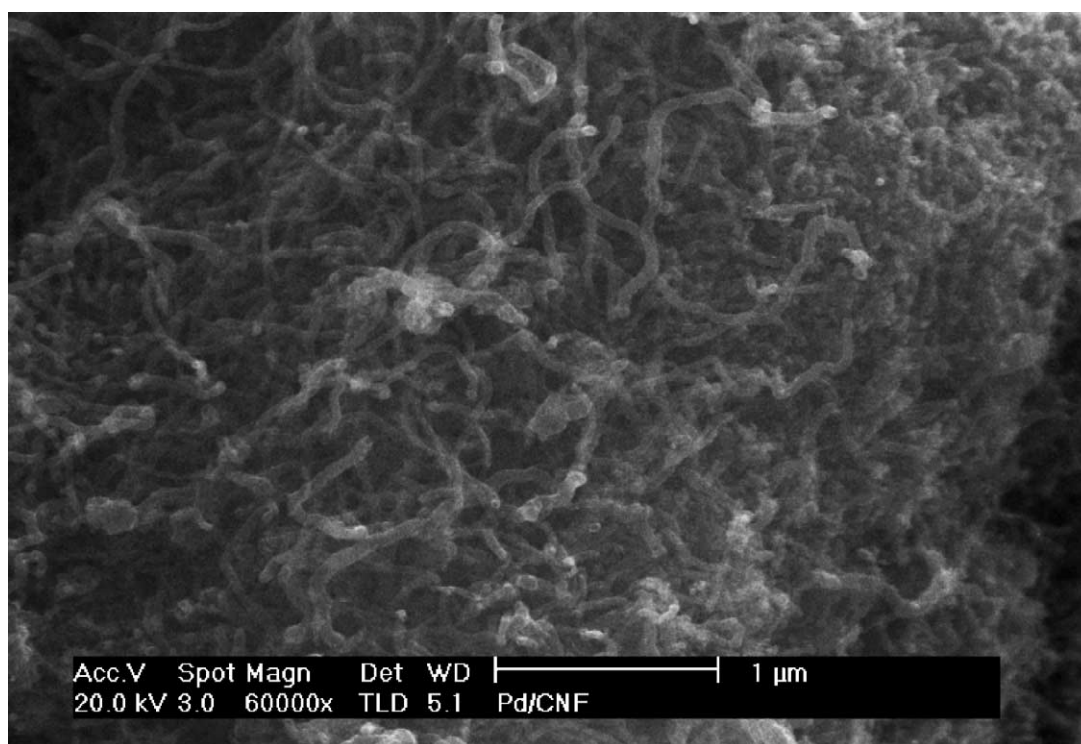


Fig. 3. SEM image of Pd/CNF.

Table 3
Characterization results for the various hydrogenation catalysts

Sample	Metal loading (wt.%)	Metal particle size (TEM, nm)	H ₂ -chemisorption		Particle size in ethanol (μm)
			H/M	d (nm)	
Pd/CNF	0.90	1–4	0.43	2.6	24
Pd/G	0.46	1–3	0.63	1.8	35
Pd/SiO ₂	2.76	1–3	0.75	1.5	23
Pt/CNF	1.24	~1	0.88	1.3	n.d.

by TEM of Pd/SiO₂ as well as of Pd/G reduced at 523 K shows small Pd particles of about 1–3 nm. Moreover, EDX analysis during TEM on Pd/G even shows Pd at surfaces where with TEM no particles are observed, indicating that also particles smaller than 1 nm must be present. Pt/CNF showed particles down to 1 nm after reduction at 473 K, but also with this sample EDX reveals the presence of smaller Pt particles. The results obtained by H₂-chemisorption for the various catalysts correspond with the results obtained by TEM analysis.

To get an indication of the macroscopic size of the catalyst particles measurements were performed after severely crushing the various catalysts and suspending them in ethanol (Table 3). Pd/CNF and Pd/SiO₂ show a volume averaged particle size of 24 and 23 μm, respectively. However, the particle size distribution is rather broad with most of the particles in the range of 2–10 μm, whereas the largest part of the volume fraction is in the range 6–30 μm. Pd/G shows a somewhat higher average particle size, i.e., 35 μm, caused by the presence of some particles larger than 70 μm. However, with this catalyst the large portion of the volume fraction can be found in the range 2–22 μm.

3.4. Condensation and dehydration to MO over HT_{act}

The catalytic properties of HT_{act} were investigated in the formation of MO from acetone at 313 K (Fig. 5). As can be seen, the condensation of acetone to DAA proceeds very rapid over HT_{act} and equilibrium (0.45 mol_{DAA} l⁻¹) is attained within the first hour. The rate of dehydration of DAA to MO is much lower. We found an initial rate in the dehydration reaction of 9.3×10^{-3} mol_{MO} g_{HT}⁻¹ h⁻¹, which is six times higher than that measured by Roelofs et al. at 296 K [2,26]. The activity in the dehydration reaction lowers somewhat in time, which is most likely due to the gradually increasing concentration of MO and water.

3.5. Hydrogenation of MO in ethanol

In Fig. 6 the results of the hydrogenation at 313 K of 0.08 mol l⁻¹ MO at 1.2 bar H₂ and 0.35 mol l⁻¹ MO at 1.2 and 10 bar H₂ over Pd/CNF are depicted. Under the given conditions this catalyst exhibits high (initial) activities and high selectivities (Table 4). The reaction with MO₀ = 0.08 mol l⁻¹ at 1.2 bar resulted in complete conversion within 40 min. Although the reaction with MO₀ = 0.35 mol l⁻¹ at 1.2 bar started with a somewhat higher rate (Table 4), probably due to the higher initial MO concentration, a decrease in rate was observed right from the start resulting in a total deactivation after about 3 h (Fig. 6). Deactivation of the catalyst, however, was avoided or at least suppressed to a large extent when the hydrogen pressure was increased up to 10 bar. From these results it may be concluded that at relatively high MO concentrations (polymerisation) products are formed which irreversibly deactivate the metal sites. A high excess concentration of

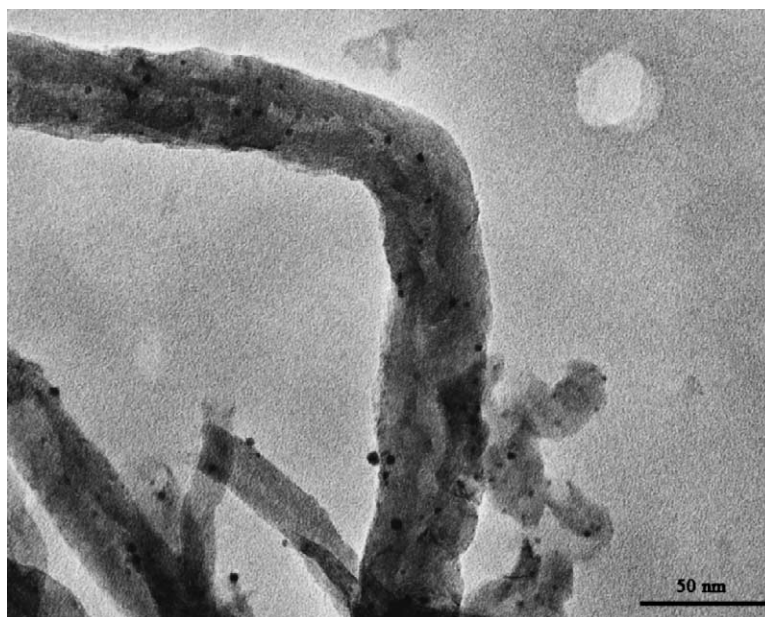
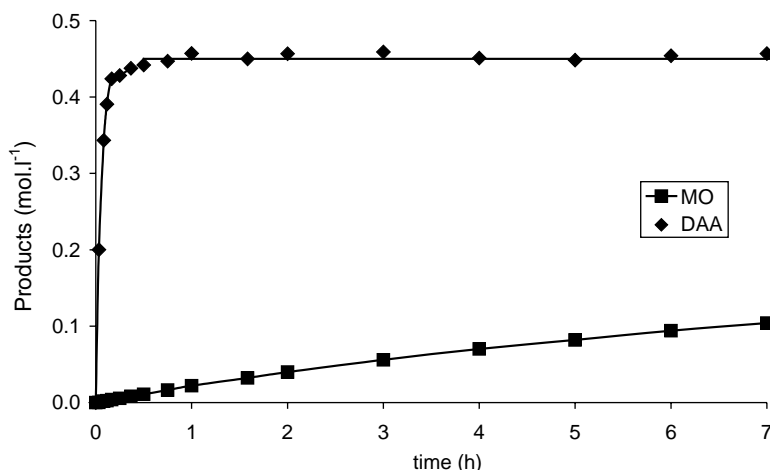
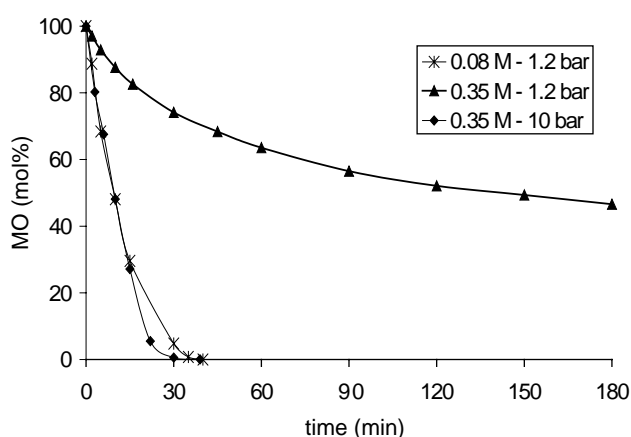


Fig. 4. TEM image of Pd/CNF after reduction at 523 K.

Fig. 5. DAA and MO production at 313 K with HT_{act}.Fig. 6. MO (0.08 and 0.35 M) hydrogenation at 1.2 and 10 bar H₂ over Pd/CNF at 313 K in ethanol.

MO at the active sites could occur if hydrogen is rapidly depleted in the catalyst particles due to a high rate of hydrogenation in combination with its low solubility.

Nijhuis et al. [39] and Ros et al. [40] exploring the use of small rhodium particles on CNF for the hydrogenation of cyclohexene, recently found that at low hydrogen pressures (~1 bar) hydrogenation reactions with comparably high reaction rates give rise to internal mass transfer limitations in hydrogen. A first indication that the MO hydrogenation at 1.2 bar hydrogen over our Pd/CNF catalyst suffers from

mass transfer limitation in hydrogen appeared from the experiments with catalyst samples, which were shortly and prolongedly crushed to obtain samples with different particle sizes. With $MO_0 = 0.08 \text{ mol l}^{-1}$ the initial reaction rate increased almost twofold with decreasing catalyst particle size. We also calculated the Weisz–Prater number (Φ) for an n th order reaction [41] that indicates the absence of internal mass transfer limitations if:

$$\Phi = \frac{\rho_p r_{w,p}^{obs} d_p^2}{36 D_e C_s} \left(\frac{n+1}{2} \right) < 0.15$$

The parameters used for the calculation of Φ (in H₂) for the reaction over Pd/CNF in ethanol as solvent at 1.2 bar H₂ are given in Table 5. We found a value for Φ of 1.3 which is amply above the value of 0.15. The initial rate when started with $MO_0 = 0.35 \text{ mol l}^{-1}$ at 10 bar is $1.11 \times 10^{-3} \text{ mol}_{MO} \text{ g}_{cat}^{-1} \text{ s}^{-1}$ and from this value, with $C_{hydrogen} = 38.3 \text{ mol m}^{-3}$ [42] and the other relevant parameters of Table 5, a value for the Weisz–Prater number of 0.66 could be derived. Obviously, although this value still exceeds the criterion and mass transfer limitation still occurs, this did not bring about deactivation. At 10 bar hydrogen is available throughout the catalyst particle thereby protecting the Pd active phase from deactivation. We cannot, however, exclude deactivation of part of the metal sites at relatively high MO concentrations, i.e., in the first stage of the reaction.

Table 4
Activity and selectivity for MO hydrogenation in ethanol

Sample	MO concentration (mol l ⁻¹)	H ₂ pressure (bar)	Initial activity × 10 ⁴ (mol _{MO} g _{cat} ⁻¹ s ⁻¹)	TOF ^a (s ⁻¹)	Selectivity to MIBK (%)
Pd/CNF	0.08	1.2	2.54	6.9	>99
	0.35	10	11.1	30.1	>99
Pd/G	0.08	1.2	0.69	2.5	>99
Pd/SiO ₂	0.08	1.2	2.84	1.5	>99
Pt/CNF	0.08	1.2	0.99	1.8	94

^a TOF is given for the first 120 s in mol MO hydrogenated, per mol metal surface atoms in the catalyst per second.

Table 5

Values of the parameters used to validate the Weisz–Prater criterion for the presence of internal diffusion limitations

Parameter		Value
$r_{w,p}^{obs}$	Observed reaction rate per unit mass of catalyst particle ($\text{mol kg}_{cat}^{-1} \text{s}^{-1}$)	0.25
d_p	Catalyst particle diameter (m)	24×10^{-6}
ρ_p	Density of catalyst particle (kg m^{-3})	1020
$C_{hydrogen}$	Concentration of reactant (mol m^{-3})	4.6
D^a	Diffusion coefficient ($\text{m}^2 \text{s}^{-1}$)	2.3×10^{-9}
ε	Void fraction of catalyst particle	0.46
τ	Tortuosity factor	2
D_e	Effective diffusion coefficient of reactant ($\text{m}^2 \text{s}^{-1}$)	7.2×10^{-10}
ϕ^b	Weisz–Prater	1.3

^a Diffusion constant is determined by using the method from Wilke-Chang [48,49].

^b Calculated with the assumption that the reaction is first order.

In Table 4 the results obtained with $\text{MO}_0 = 0.08 \text{ mol l}^{-1}$ at 313 K and 1.2 bar H_2 for all four catalysts are given. Pt/CNF exhibits a comparable activity in the hydrogenation of MO as the palladium catalysts, however, with a selectivity significantly lower than measured with the palladium catalysts of 94 and >99%, respectively. Although the reaction is restricted by mass transfer of H_2 , the average catalyst particle size of all catalysts is rather similar making an exploratory study on their performances meaningful. Pd/CNF exhibits an initial activity 3-fold that of Pd/G and an activity rather similar to that obtained with Pd/ SiO_2 . Comparison of the turn over frequencies (TOF) obtained with these catalysts shows the distinct activity of Pd/CNF to be even more pronounced. The TOF obtained with Pd/CNF is a factor 3 and 5 higher than these obtained with Pd/G and Pd/ SiO_2 , respectively. The reason for this difference can be the effect of the presence of oxygen-containing surface groups on the carbon support [43–45] or of the metal particle size [46]. However, the metal particle sizes do not differ significantly. As was already stated by Toebes et al. [45,47], oxygen containing

surface groups on the carbon nanofibers can have a tremendous effect on the activity and selectivity in hydrogenation reactions. It could well be that the presence of these functional groups introduced by treatment in nitric acid, results in a more active catalyst. More research is needed to fully elucidate these effects, preferentially without the presence of mass transfer limitations in H_2 enabling comparison between the intrinsic activities of the catalysts more quantitatively.

3.6. Hydrogenation of MO in acetone

In order to investigate to what extent the hydrogenation of MO under mild conditions over these catalysts is applicable in the single-stage process of MIBK starting from acetone and hydrogen, hydrogenation experiments were performed in acetone as solvent and reactant. Hydrogenation of $\text{MO}_0 = 0.08 \text{ mol l}^{-1}$ in acetone over Pd/CNF did not bring about acetone hydrogenation up to 20 bar over Pd/CNF. Moreover, the selectivity of the hydrogenation of MO to MIBK remained >99%.

However, concerning deactivation very different results were obtained when the hydrogenation with $\text{MO}_0 = 0.08 \text{ mol l}^{-1}$ was performed at 1.2 bar H_2 in acetone instead of in ethanol. Hydrogenation at 1.2 bar H_2 led to a rapid deactivation of all catalysts (Fig. 7). A side reaction of MO in which acetone might be involved, because with $\text{MO}_0 = 0.08 \text{ mol l}^{-1}$ in ethanol this fast deactivation does not occur. In a next experiment it was tested whether acetone itself deactivates the catalyst. To this end the catalyst was suspended in acetone at 1.2 bar H_2 one hour before adding MO. It turned out that the catalyst was still active, which demonstrates that probably polymerisation of MO and/or a reaction of MO with acetone cause deactivation. It is clear that this deactivation is not just a feature of the carbon supported catalysts, since hydrogenating MO under these conditions over Pd/ SiO_2 results in deactivation too (Fig. 7).

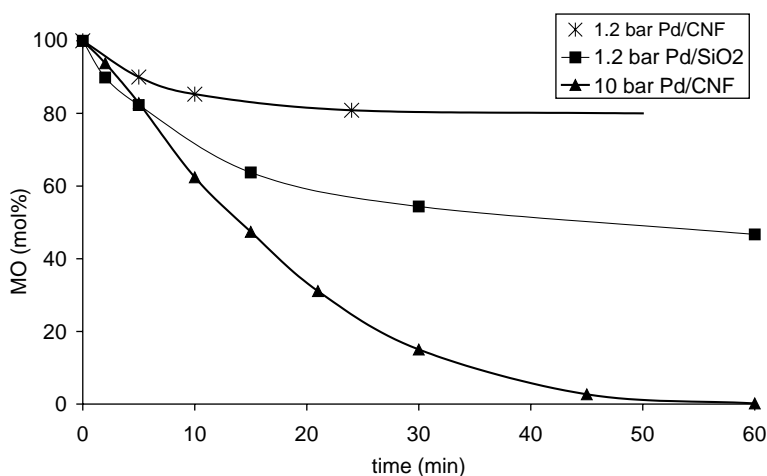


Fig. 7. MO (0.08 mol l^{-1}) hydrogenation at 313 K in acetone at 1.2 and 10 bar H_2 over Pd/CNF and at 1.2 bar H_2 over Pd/ SiO_2 .

The activity of Pd/CNF is maintained when a hydrogen pressure as high as 10 bar is applied and full conversion is obtained, which demonstrates that a rapid decrease of the MO concentration or a good availability of hydrogen throughout the catalyst particles is needed to avoid deactivation. The initial rate observed at 10 bar H₂ over Pd/CNF was found to be $1.5 \times 10^{-4} \text{ mol}_{\text{MO}} \text{ g}_{\text{cat}}^{-1} \text{ s}^{-1}$ and a Weisz–Prater number of 0.04 was calculated, indicating the absence of mass transfer limitations in H₂ when performing the reaction in acetone at 10 bar H₂.

3.7. Combination of Pd/CNF and HT_{act} in the single-stage production of MIBK

The suitability of a mixture of HT_{act} and Pd/CNF in the single-stage process of MIBK starting from acetone and H₂ was tested at 1.2 bar H₂ and 331 K (Fig. 8). In Table 6 the activity and TOF values over the first 30 min in the condensation, dehydration and hydrogenation reaction are given. The rate of the dehydration reaction is calculated from the sum of the amount of MIBK and the amount of MO formed during reaction. At this reaction temperature, the condensation reaction of acetone to form DAA proceeds extremely fast as equilibrium is attained within 5 min. The rate of condensation over HT_{act} was calculated to be $1.3 \text{ mol}_{\text{DAA}} \text{ g}_{\text{HT}}^{-1} \text{ h}^{-1}$ (Table 6) over the first minutes and the DAA concentration stayed at equilibrium throughout the experiment.

During the experiment the MO concentration remained low at a value of 0.003 mol l^{-1} by further hydrogenation to MIBK. Within the first three hours the productivity of the catalyst system decreased somewhat, but next a stable MIBK production rate was found for several hours. Deactivation of the hydrogenation catalyst was not apparent, which is due to the low steady-state concentration of MO during the experiment even at this low H₂ pressure. The dehydration rate over HT_{act} after three hours was found to be $6.2 \times 10^{-3} \text{ mol}_{\text{MO}} \text{ g}_{\text{HT}}^{-1} \text{ h}^{-1}$, with a selectivity to the desired products (DAA, MO and MIBK) of around 95%. The main side products are due to secondary condensations as was

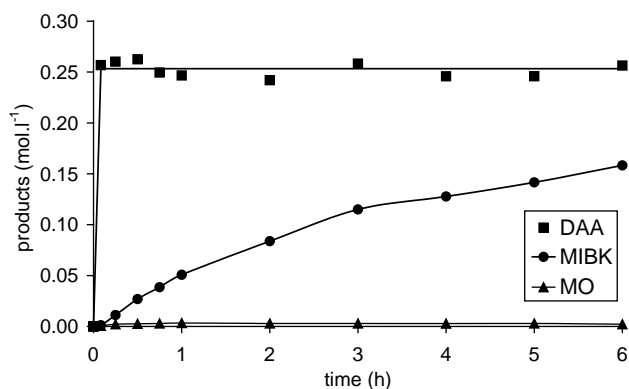


Fig. 8. Formation of DAA, MO and MIBK in the single-stage liquid-phase synthesis of MIBK from acetone and H₂ (1.2 bar) at 331 K over 0.3 g HT_{act} and 0.2 g Pd/CNF in 1.8 mol acetone.

Table 6

Activity and TOF for the single-stage production of MIBK over a catalyst mixture of HT_{act} and Pd/CNF at 331 K and 1.2 bar H₂

	Activity ^a (mol product g _{HT} ⁻¹ h ⁻¹)	TOF ^a (s ⁻¹)
DAA production	1.34 [#]	1.26 [#]
MO production	0.026	0.024
MIBK formation	0.023	0.022

^a Activity and TOF calculated over the first 30 min or when marked with (#) over the first 5 min over HT_{act}. Activity and TOF in the MIBK formation over Pd/CNF are $0.036 \text{ mol}_{\text{MIBK}} \text{ g}_{\text{pd/cnf}}^{-1} \text{ h}^{-1}$ and 0.27 s^{-1} , respectively.

found with GC-MS, which could, together with water, affect the catalytic activity of HT_{act}. It was investigated separately whether the Pd/CNF displays any dehydration functionality. It was found that under these conditions the dehydration reaction proceeds exclusively over HT_{act}.

It appears that after three hours the reaction is in pseudo steady-state, as the MO concentration did not increase during the course of the reaction and the MIBK production rate remained constant. These observations strongly indicate that the production rate of MIBK is mainly determined by the rate of dehydration. Furthermore, the TOF in the MIBK formation over Pd/CNF is about 10-fold the TOF in the dehydration over HT_{act} (Table 6).

From the arguments mentioned above we can conclude that most likely the dehydration reaction over HT_{act} is the rate-determining step in the single-stage synthesis of MIBK under the described mild conditions. Above results show the potential of this catalyst system for the single-stage liquid-phase synthesis of MIBK from acetone and hydrogen under mild conditions. Note that the system is far from optimised. Further work will concentrate on the condensation and dehydration reaction over activated hydrotalcites in order to improve the MIBK productivity of this catalyst system.

4. Conclusions

Results obtained with the HT_{act}-Pd/CNF catalyst mixture demonstrate the suitability of this catalyst system for the single-stage liquid-phase production of MIBK from acetone and hydrogen under mild conditions. Due to the balance between the formation rate of MO and the rate of its hydrogenation, from the start the steady state concentration of MO is low and remains low even at a hydrogen pressure as low as 1.2 bar, due to which deactivating species starting from MO are not formed. The catalytic activity is stable over several hours. In this process dehydration of DAA to MO over HT_{act} is rate limiting.

Acknowledgements

The authors are grateful to C. van der Spek, V. Koot, A. Mens and M. Versluijs-Helder for their technical assistance.

P. Groenendijk (DOW) is kindly thanked for helping perform the catalysis measurements at higher pressures. The Netherlands Technology Foundation (CW/STW 790.35.733) is acknowledged for financial support.

References

- [1] G.G. Podrebarac, F.T.T. Ng, G.L. Rempel, *Chem. Eng. Sci.* 52 (1997) 2991.
- [2] J.C.A.A. Roelofs, PhD thesis, Utrecht University, The Netherlands, 2001.
- [3] Y.K. Kim, J.D. Hatfield, *J. Chem. Eng. Data* 30 (1985) 149.
- [4] E.C. Craven, *J. Appl. Chem.* 13 (1963) 71.
- [5] C.U. Pittman Jr., Y.F. Liang, *J. Org. Chem.* 45 (1980) 5048.
- [6] D. Bombos, Gr. Bozga, M. Bombos, A. Stefan, I. Stanciu, *Rom. Chem. Papers* 54 (2000) 171.
- [7] L. Melo, G. Gianetto, F. Alvarez, P. Magnoux, M. Guisnet, *Catal. Lett.* 44 (1997) 201.
- [8] P.Y. Chen, S.J. Chu, W.C. Lin, K.C. Wu, C.L. Yang, *Stud. Surf. Sci. Catal.* 83 (1994) 481.
- [9] Y.Z. Chen, B.J. Liaw, H.R. Tan, K.L. Shen, *Appl. Catal. A: Gen.* 205 (2001) 61.
- [10] Y. Higashio, T. Nakayama, *Catal. Today* 28 (1996) 127.
- [11] L.M. Gandia, M. Montes, *J. Mol. Catal.* 43 (1994) 347.
- [12] L.M. Gandia, M. Montes, *Appl. Catal. A: Gen.* 101 (1993) L1.
- [13] K.H. Lin, A.N. Ko, *Appl. Catal. A: Gen.* 147 (1996) L259.
- [14] G.S. Salvapati, K.V. Ramanamurty, M. Janardanao, *J. Mol. Catal.* 54 (1989) 9.
- [15] A.A. Nikolopoulos, G.B. Howe, B.W.-L. Jang, R. Subramanian, J.J. Spivey, D.J. Olsen, T.J. Devon, R.D. Culp, in: M.E. Ford (Ed.), *Chemical Industries, Catalysis of Organic Reactions*, vol. 82, New York, 2001, p. 533.
- [16] A.A. Nikolopoulos, B.W.-L. Jang, R. Subramanian, J.J. Spivey, D.J. Olsen, T.J. Devon, R.D. Culp, *ACS Symposium Series 767 (Green Chemical Processes)*, Charleston, 2000, p. 194.
- [17] S. Lippert, W. Baumann, K. Thomke, *J. Mol. Catal.* 69 (1991) 199.
- [18] Y.Z. Chen, B.J. Liaw, H.R. Tan, K.L. Shen, *Appl. Catal. A: Gen.* 169 (1998) 207.
- [19] N. Das, D. Tichit, R. Durand, P. Graffin, B. Coq, *Catal. Lett.* 71 (2001) 181.
- [20] R. Unnikrishan, S. Narayanan, *J. Mol. Catal. A: Chem.* 144 (1999) 173.
- [21] K.K. Rao, M. Gravelle, J. Sanchez-Valente, F. Figueras, *J. Catal.* 173 (1998) 115.
- [22] D. Tichit, M.H. Lhouty, A. Guida, B. Chiche, F. Figueras, A. Auroux, D. Bartalini, E. Garrone, *J. Catal.* 151 (1995) 50.
- [23] D. Tichit, M.N. Benanni, F. Figueras, R. Tessier, J. Kervennal, *Appl. Clay Sci.* 13 (1998) 401.
- [24] A. Guida, L.M. Hassane, D. Tichit, F. Figueras, P. Geneste, *Appl. Catal. A: Gen.* 164 (1997) 251.
- [25] J.C.A.A. Roelofs, D.J. Lensveld, A.J. van Dillen, K.P. de Jong, *J. Catal.* 203 (2001) 184.
- [26] J.C.A.A. Roelofs, A.J. van Dillen, K.P. de Jong, *Catal. Today* 60 (2000) 297.
- [27] M.L.A. von Holleben, M. Zucolotto, C.A. Zini, E.R. Oliveira, *Tetrahedron* 50 (1994) 973.
- [28] J. Wisniak, M. Herskowitz, D. Roffe, S. Smilovitz, *Ind. Eng. Chem. Prod. Res. Dev.* 15 (1976) 163.
- [29] A. Alba, M.A. Aramendia, V. Borau, C. Jimenez, J.M. Marinas, *React. Kinet. Catal. Lett.* 25 (1984) 45.
- [30] V. Ponc, *Appl. Catal. A: Gen.* 149 (1997) 27.
- [31] K.P. de Jong, J.W. Geus, *Catal. Rev. -Sci. Eng.* 42 (2000) 481.
- [32] S. Miyata, T. Kumura, *Chem. Lett.* (1973) 843.
- [33] J.C.A.A. Roelofs, A.J. van Dillen, K.P. de Jong, *Catal. Lett.* 74 (2001) 91.
- [34] M.L. Toebes, J.M.P. van Heeswijk, J.H. Bitter, A.J. van Dillen, K.P. de Jong, *Carbon* 42 (2004) 307.
- [35] M.L. Toebes, J.H. Bitter, A.J. van Dillen, K.P. de Jong, *Catal. Today* 76 (2002) 33.
- [36] M.S. Hoogenraad, Ph.D. thesis, Utrecht University, The Netherlands, 1995.
- [37] T.G. Ros, Ph.D. thesis, Utrecht University, The Netherlands, 2002.
- [38] W.T. Reichle, S.Y. Kang, D.S. Everhardt, *J. Catal.* 101 (1986) 352.
- [39] T.A. Nijhuis, G. van Koten, F. Kapteijn, J.A. Moulijn, *Catal. Today* 79/80 (2003) 315.
- [40] T.G. Ros, D.E. Keller, A.J. van Dillen, J.W. Geus, D.C. Koningsberger, *J. Catal.* 211 (2002) 85.
- [41] R.A. van Santen, P.W.N.M. van Leeuwen, J.A. Moulijn, B.A. Averill, *Catalysis: An integrated Approach*, Second, Revised and Enlarged Edition, Elsevier, Amsterdam 2nd edition, 1999 pages.
- [42] C.L. Young, *Solubility Data Series*, vol. 5/6, Hydrogen and Deuterium, Pergamon Press, Oxford, 1981.
- [43] H.P. Boehm, *Carbon* 32 (1994) 759.
- [44] S.S. Barton, M.J.B. Evans, E. Halliop, J.A.F. MacDonald, *Carbon* 35 (1997) 1361.
- [45] M.L. Toebes, Ph.D. thesis, Utrecht University, The Netherlands, 2004.
- [46] B. Coq, F. Figueras, *Coord. Chem. Rev.* 178/180 (1998) 1753.
- [47] M.L. Toebes, F.F. Prinsloo, J.H. Bitter, A.J. van Dillen, K.P. de Jong, *J. Catal.* 214 (2003) 78.
- [48] R.H. Perry, D.W. Green, *Perry's Chemical Engineers' Handbook*, McGraw-Hill, 7th edition, New York, 1997.
- [49] C.R. Wilke, P. Chang, *AIChE J.* (1955) 264.